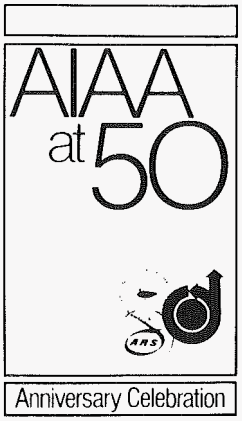

AIAA-81-1245 Investigation of Strong Shock Turbulent Boundary Layer Interaction in 2-D Transonic Flows with Emphasis on Turbulence Phenomena

J. M. Delery, ONERA, Chattillon, France

AIAA 14th Fluid and Plasma Dynamics Conference

June 23-25, 1981/Palo Alto, California

INVESTIGATION OF STRONG SHOCK 'TURBULENT BOUNDARY LAYER INTERACTION IN 2D TRANSONIC FLOWS WITH EMPHASIS ON TURBULENCE PHENOMENA("")

J.M. DELERY"

A81-38099

OFFICE NATIONAL D'ETUDES ET DE RECHERCHES AEROSPATIALES,
29 Avenue de la Division Leclerc, 92320 CHATILLON (France)

Abstract

Three flows resulting from shock wave turbulent boundary layer interactions occurring in a 2D-transonic channel have been investigated. The first flow corresponds to incipient shock induced separation, the second to a neatly separated case, the third to a situation where a large separated bubble forms. The flows were characterized by using two-color laser velocimetry and holographic interferometry. The results include Mach number contours for the inviscid part of the most separated flow and, for the three flows, mean velocity and Reynolds stress distributions across the viscous layer. The turbulence measurements reveal that the first part of the interaction process entails a very large turbulence production with the development of a very strong anisotropy. In this zone, the neglect of normal shear stress in the momentum and turbulence energy equation is not justified. The downstream relaxation towards a new equilibrium state is a very gradual process due to the long life-time of the large structures which formed in the region of intense turbulence production.

Nomenclature

a : speed of sound
b : conventional mixing zone thickness
C_τ : maximum shear stress coefficient, $2\tau/\rho_e u_e^2$
H_i : incompressible shape parameter
J : equilibrium shape parameter, $1 - 1/H_i$
k : turbulent kinetic energy $1/2\ (\langle u' \rangle^2 + \langle v' \rangle^2 + \langle w' \rangle^2)$
l : Prandtl mixing length
M : Mach number
p : pressure
R : reattachment point
R_θ : Reynolds number based on momentum thickness
S : separation point
T : absolute temperature
u : velocity component in streamwise direction
v : velocity component in normal direction
w : velocity component in cross-stream direction
X : coordinate in the streamwise direction
$\tilde{X}$: reduced streamwise coordinate, $(X - X_0)/(\delta_0^*)$
Y : coordinate in the normal direction
δ : dissipative layer thickness
δ^* : displacement thickness
θ : momentum thickness
φ : dimensionless velocity
ρ : fluid density
τ : Reynolds shear stress, $-\rho\ \overline{u'v'}$

Subscripts

e : edge of dissipative layer
t : stagnation condition
o : origin of interaction

Superscripts

' : fluctuating quantity
- : time-averaged quantity
$\langle\ '\ \rangle$: RMS value of quantity.

Introduction

Viscous effects play a major role in transonic flows where they can strongly affect the whole flowfield. This problem is specially important in supercritical flows where the strong viscous interaction occurring near the shock root entails a rapid thickening of the boundary layer and can lead to its separation if the shock is strong enough. These phenomena are encountered in many domains of practical interest : wings and airfoils, turbomachines, helicopter blades,... This fact explains the sustained effort to develop accurate predictive methods able to cope with this very difficult problem. Two kinds of approaches are followed at the moment :

- Interaction techniques where an inviscid external flowfield and dissipative layers (boundary layers and/or wakes) are computed separately and made compatible through matching conditions. In these techniques, the dissipative layers are frequently computed by integral methods applied to boundary layer type equations. These procedures have achieved some success, even in the case of moderately separated flows, with relatively short computer time[1].
- Numerical solution of the full Navier-Stokes equations, which seem the most appropriate procedure to predict the flow structure in regions where the use of the Prandtl's equation is questionable. (shock root, separation region, trailing edge).

Considerable advances have been made in the development of efficient and accurate numerical codes which solve the Navier-Stokes equations. But the numerous and systematic applications made in transonic and/or supersonic flows involving Shock Wave-Turbulent Boundary Layer Interaction (SW-TBLI) have frequently led to very poor agreement with experiment, especially when separation occurs[2,3,4,5,6]. This inability to accurately account for viscous effects is primarily due to the deficiencies of the models employed to describe the turbulence properties of the flow. In fact, all the models tested (algebraic as well as multi-equation models) are appropriate for boundary layers undergoing relatively weak pressure gradients and, for this reason, are unable to cope with the very strongly out of equilibrium conditions typical of a shock induced separation. To define more realistic turbulence models, precise quantitative measurements of the turbulence properties are needed.

The experimental analysis of a SW-TBLI is a rather delicate task due to the sensitivity of the flow to disturbing effects. In the past few years, much valuable information has been obtained by using pressure probes'.'. But the data thus obtained are not free of disturbances introduced by the probes, especially when separation occured. Furthermore, they do not give any information about turbulence. The use of quantitative interferometry constituted a first

"Division Deputy Head

(••) Thisresearch wav made with the financial support of the Directiondes Recherches et Etudes Techniques and of the Service Technique des Programmes Aéronautiques of the French Defence Ministry.

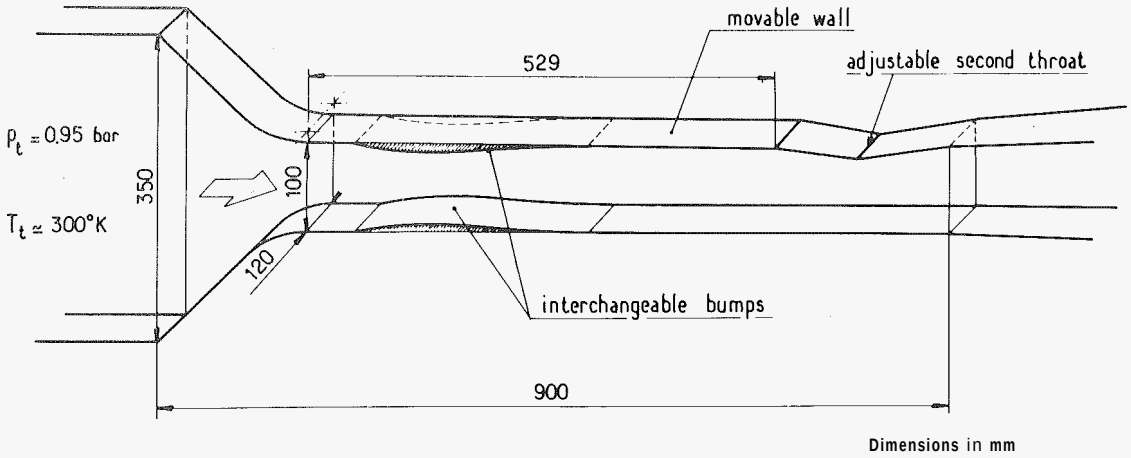

Fig. 1 – Experimental arrangement.

improvement of the experimental methods, since this technique is non-intrusive[9,10] and can give a large amount of information about the mean flow structure. However, interferometry is unable to make local turbulence measurements. This gap was filled by the relatively recent advent of Laser Doppler Velocimetry which makes it possible to measure the turbulence properties in complex aerodynamic flows. Very valuable results concerning supersonic as well as transonic flows have already hsen published[11,12,13,14]. So, it is now possible to closely couple experiment and computation in order to develop more exact turbulence models.

This paper presents data on three SW-TBLI produced in a transonic channel flow and ranging from incipient shock induced separation situation to largely separated flow condition. The data consist of mean velocity and Reynolds stress components obtained with a two-color Laser Velocimeter.

Experimental technique

The experiments were conducted in the S8 transonic channel of the ONERA Fluid Mechanics Laboratory. This wind tunnel is continuously supplied with dessicated atmospheric air, the stagnation conditions being as follows : pressure p_t = 0.95 bar, temperature : T_t = 300°K. The test section, shown in Fig. 1, has a span equal to 120 mm and an entrance height of 100 mm. Interchangeable nozzle blocks or bumps can be mounted in the working section with a view to accelerating the flow up to slightly supersonic velocities. A second throat, of adjustable cross section, is placed at the test section outlet making it possible :

- to produce, by choking effect, a shock wave whose position, and hence intensity, can be adjusted in a continuous and precise manner,
- to isolate the flowfield under study from pressure perturbations emanating from downstream ducts. Such a device notably reduces shock oscillations.

The SW-TBLI phenomena under investigation take place on the lower wall of the channel at a station where the undisturbed turbulent boundary layer has a thickness δ_0 of several millimeters (from 3 to 5 mm)

Laser Velocimeter

Mean and fluctuating velocity measurements were made with a two-color laser velocimeter developed at ONERA. A schematic of the system arrangement is shown in Fig. 2. The apparatus uses the fringe mode of operation. The light source is a 15-W argon laser whose beam is separated into two beams of 0.488 μm and 0.5145 μm wavelength by the dichroic mirror M_D. The two original beams are first split and then traverse Bragg cells to enable the system to detect the velocity direction by causing the fringes forming in the probe volume to move at a shifting frequency which can be varied from 0 to 8 MHz. The four beams are focused by the emission lens to constitute the measuring volume whose diameter is approximately equal to 300 μm. The two fringe patterns are rotated at ± 45°. allowing the simultaneous measurement of two velocity components in a vertical plane.

The two photomultipliers, collecting the forward scattered light, are preceded by interferential filters. The whole system is mounted on a very rigid table allowing precise and automated displacements along three orthogonal axes. The data acquisition and processing unit comprises, as main elements, two laser Doppler signal processors (DISA type 55L counters) connected to a mini-cumputer. At every measuring point, the computer performs the calculation of the statistical moments and velocity correlation from a sample of several thousand of instantaneous velocity measurements. Two-dimensional histograms are also constructed. The seeding of the flow was essentially provided by particles emanating from the dryer. Their size,

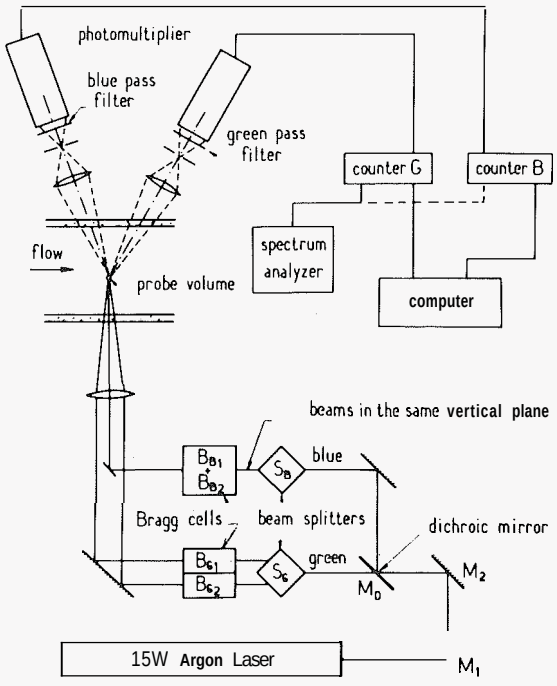

Fig. 2 – Schematic arrangement of the laser velocimeter system.

which has been carefully checked, was less than 0.4 μm. No correction for velocity biasing was applied, a previous study[**] having shown that the use of the weighting factor suggested in Ref 16 did not lead to significant differences. All the present measurements were made in the vertical plane of symmetry of the test section.

Holographic interferometer

The holographic interferometer described in Ref 17 was used to precisely define the inviscid mean flow structure associated with the interaction leading to the largest separation. The apparatus uses the double exposure technique. The finite fringe mode of operation was employed in order to increase the number of measuring points. The values of the local density were obtained from a very precise fringe pinpointing made by a microdensitometer connected to a mini-computer.

Results and discussion

Mean flow properties

Three SW-TBLIs, considered as typical, have been analysed. The corresponding distributions of the "wall" Mach number Mw are plotted in Fig. 3 (Mw is computed from wall pressure measurements assuming an isentropic relationship and considering the stagnation pressure as constant and equal to its upstream value. The reduced streamwise distance $\tilde{X}$ is evaluated from the start of interaction X_0 and scaled to the boundary layer displacement thickness at X_0). In Fig. 3 are also indicated the locations of the transverse explorations made across the dissipative layer.

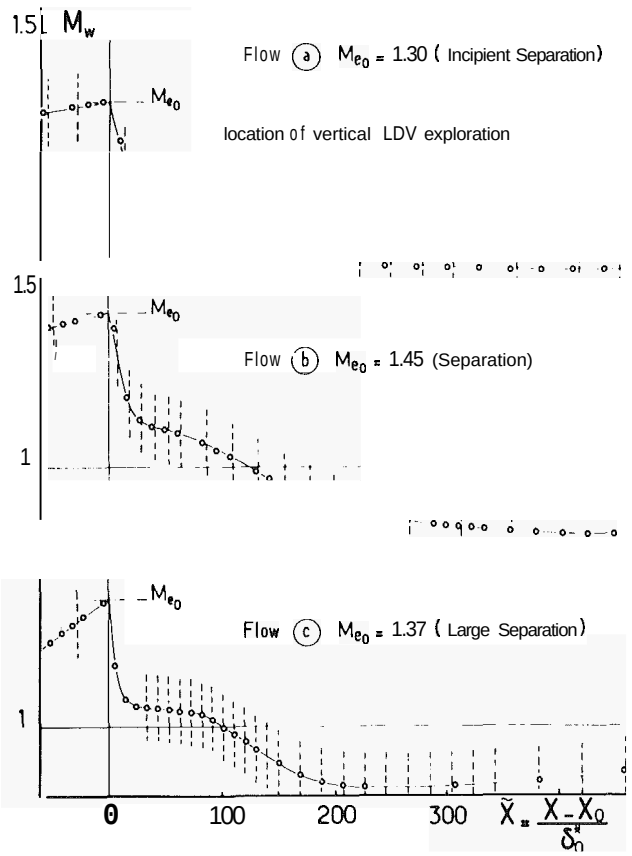

Fig. 3 – "Wall" Mach number distributions.

Flow a. Interaction corresponding to Incipient shock induced Separation (Me_0 = 1.3. IS)

For this case, the test section was equipped with a symmetrical converging-diverging supersonic nozzle whose contour was designed to produce a uniform flow having a nominal Mach number equal to 1.4. The quasi normal shock wave is situated near the end of the diverging part of the nozzle at a station where the Mach number Me_0, at the boundary layer edge, is equal to 1.30. The main global characteristics of the boundary layer at X_0 are the following :

displacement thickness : δ_0^* = 0.36 mm
momentum " : θ_0 = 0.14 mm
incompressible shape parameter : Hia = 1.30.

The Reynolds number $\mathcal{R}_{\theta_0}$, computed with the local flow conditions at X_0 and with $, has the value : $\mathcal{R}_{\theta_0}$ = 2400.

The values of Me_0 and Hi_0, in the present case, correspond to a situation which nearly coincide with incipient shock induced separation[**].

Flow b. Interaction with separation (Me_0 = 1.45 S)

Now, the supersonic flow is produced by a symmetrical nozzle having a nominal Mach number of 1.6. The shock wave is at a location in the nozzle leading to a Mach number Me_0 at the start of interaction equal to 1.45, thus a rather large separated bubble is formed. The characteristics of the boundary layer at X_0 are : δ_0^* = 0.44 mm, θ_0 = 0.18 mm, Hi_0 = 1.30. The local Reynolds number is $\mathcal{R}_{\theta_0}$ = 2500.

Flow c. *Interaction with extended separation (Me_0 = 1.37 LS)*

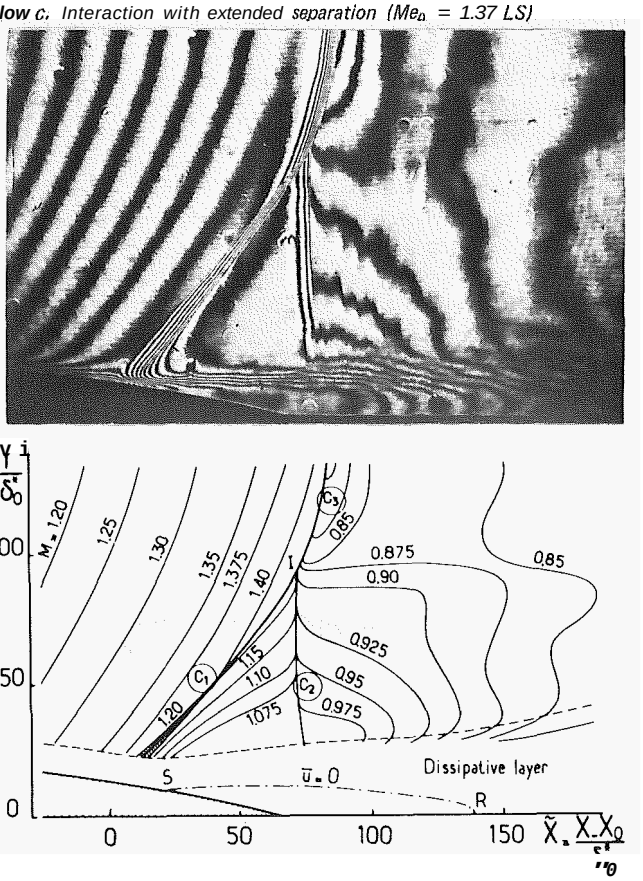

Fig. 4 – Inviscid flowfield structure–flow C.

Here, the transonic flow is produced in an asymmetrical channel where a bump is mounted on the lower wall of the wind tunnel test section (the geometrical definition of this bump can be found in Ref

15). The shock wave takes place at a location where the maximum Mach number in the flow is equal to 1.42. The situation at the origin of interaction is characterized by the values : M_{e_0} = 1.37, δ_0^* = 0.52 mm, θ_0 = 0.27 mm, H_{i_0} = 1.27 and $\mathcal{R}_{\theta_0}$ = 3800. The shock is strong enough to induce boundary layer separation upstream of the bump trailing edge. **An** extended separation bubble forms due to the wall curvature effect as is evidenced by the plateau of the wall pressure distribution. The inviscid flow structure has been carefully documented by using holographic interferometry. In Fig. **4,** Mach number contour plots obtained from a finite fringe interferogram are presented with an infinite fringe interferogram which gives a more vivid visualization of the whole flowfield. The lambda structure of this configuration is typical :

- the rapid pressure rise associated with separation gives rise to compression waves which coalesce into an oblique shock C_1 ;
- the inviscid supersonic flow region downstream of C_1 is terminated by a quasi-normal shock C_2, which is in **fact** a **strong** oblique shock ;
- shocks C_1 and C_2 meet at the bifurcation point I, from which a strong oblique shock C_3 starts.

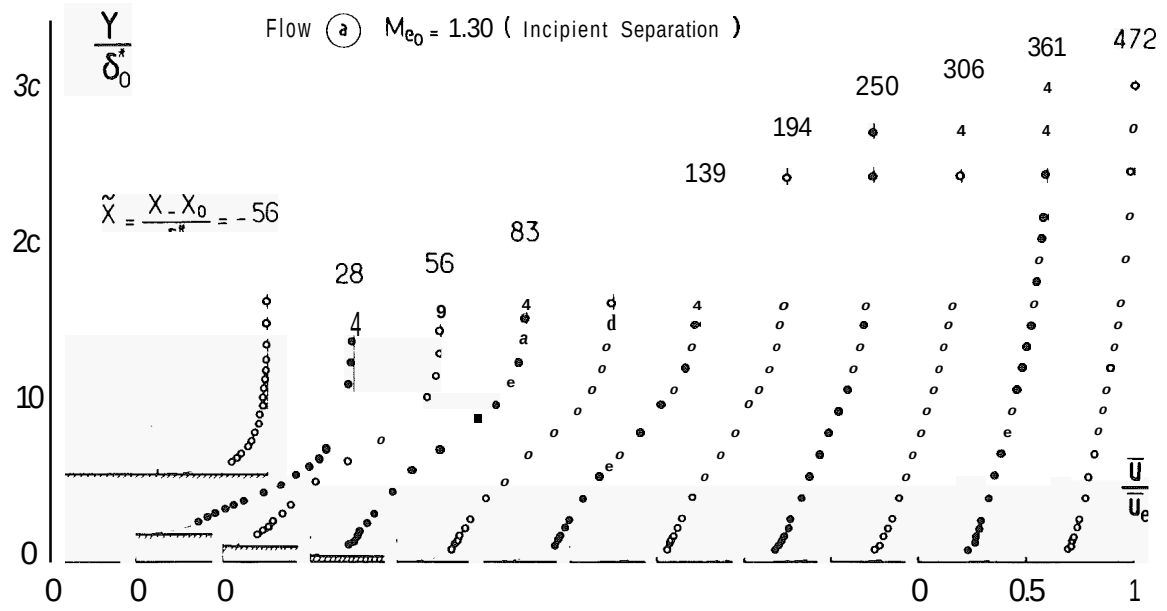

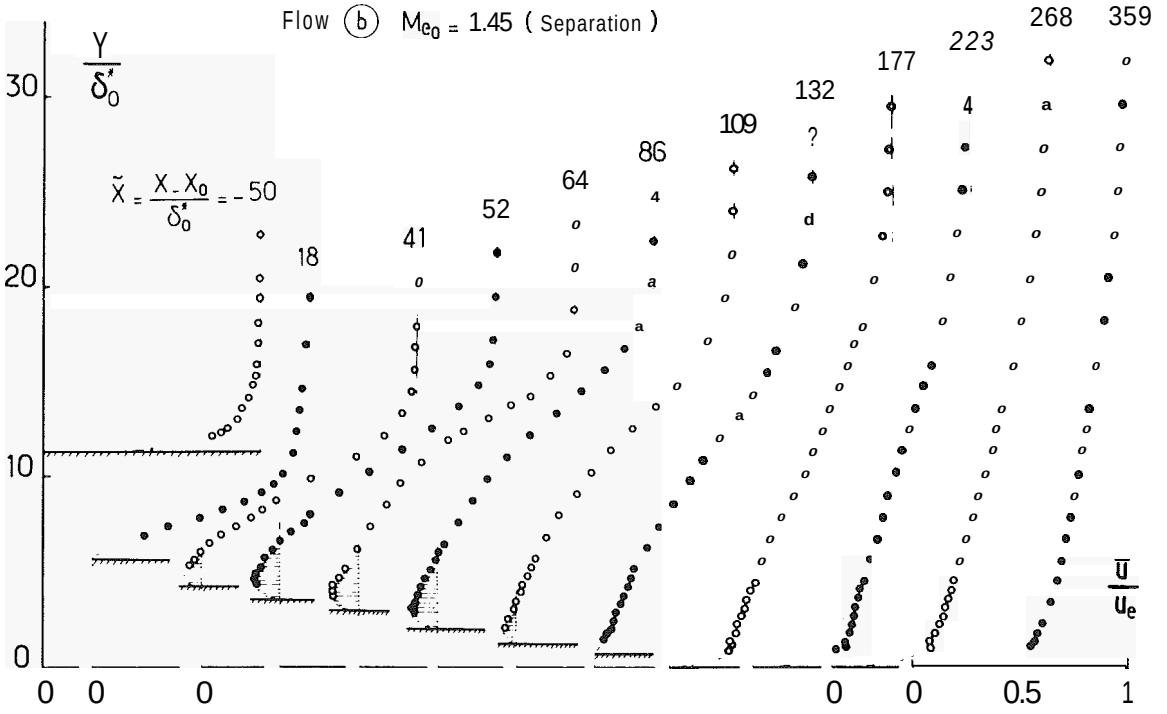

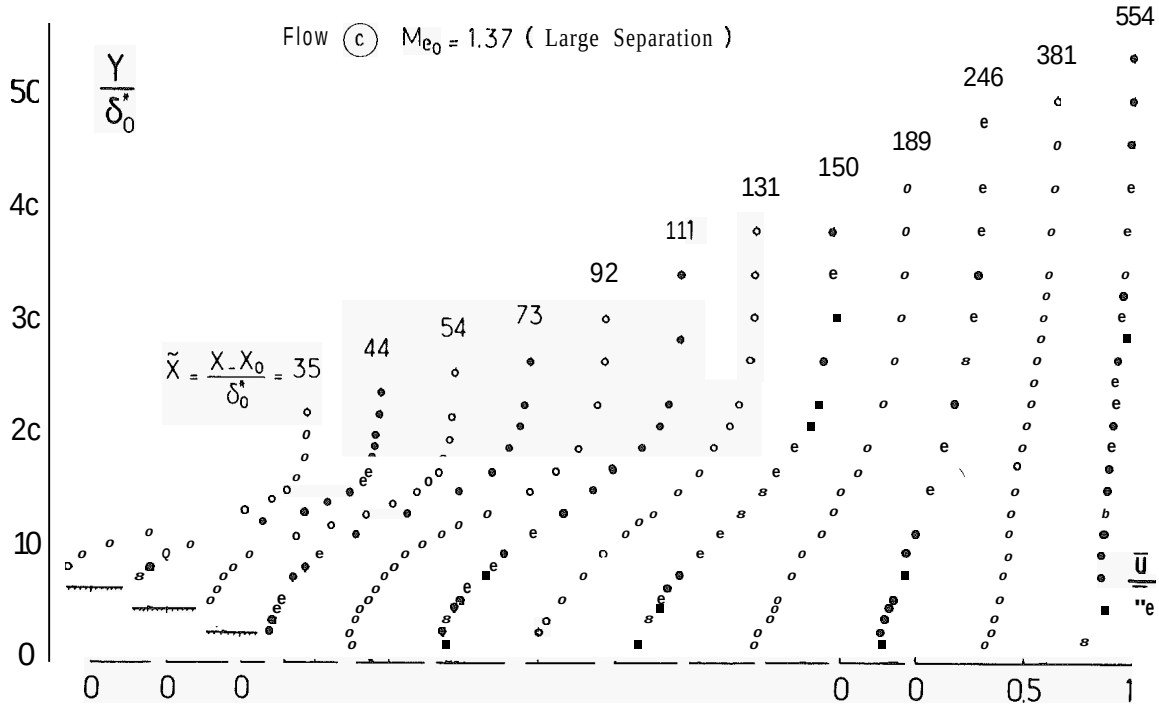

Fig. 5 – Mean streamwise velocity profiles.

It is to be noted that the boundary layer separation phenomenon is essentially a supersonic process of free interaction type, according to the concept introduced by Chapman et al.[19].

There is a fair agreement between the experimental pressure plateau and the level predicted by Chapman's theory[15]. Inviscid supersonic conditions at the edge of a largely separated boundary layer were also observed by Seegmiller et al.[12] in the case of a transonic airfoil.

Some of the mean streamwise velocity profiles measured across the dissipative layers are shown in Fig. 5. Here Y is the distance from the horizontal plane which contains the flat downstream part of the test section wall. The streamwise component $\bar{u}$ is scaled to the value of $\bar{u}$ at the boundary layer edge. The bump surface has been sketched on the figures and the profiles extrapolated to the wall value by a broken line, which is only a visual aid.

For flow a (Incipient Separation). one observes, at first, a strong destabilization of the profiles,,which entails an important decrease of $\bar{u}$ in the vicinity of the wall ; yet, no negative mean values were measured. If separation actually occurs, it concerns a very small fraction of the flow close enough to the wall for not being detected by the present measurements. The maximum retardation effect is observed at station $\tilde{X}$ = **56** ; downstream, turbulent viscous forces entail a gradual acceleration of the fluid in the inner part of the boundary layer. The thickness δ of the boundary layer is continuously increasing during the whole process.

In flow b (Separation), a noticeable reversed flow region is formed which extends from $\tilde{X}$ = **18** to $\tilde{X}$ = **132.** The thickening of the dissipative layer is now much more important than in the previous case.

In the third configuration (Large Separation), a large separated bubble exists with a maximum reduced negative velocity approximately equal to **0.2.** The length of the bubble is comparable to the length of bubble in case b, but its normal extent is here much more important (note the change in vertical scale in Fig. 5c). In this case, one observes

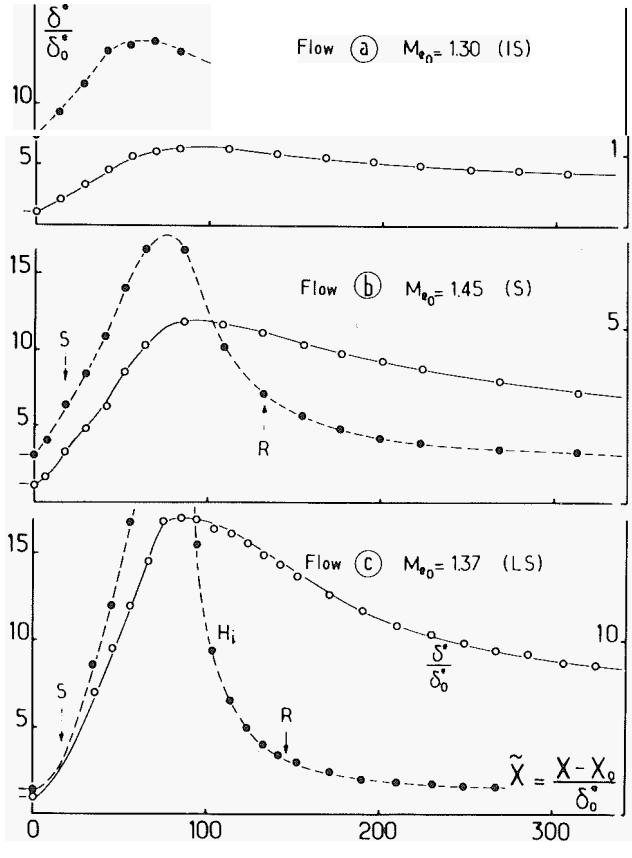

Fig. 6 – Displacement thickness and incompressible shape parameter distributions.

a dramatic increase of the boundary layer thickness, which is practically multiplied by ten between X_0 and the most downstream measuring station.

The two flows b and c lead to profiles whose shape and behavior in the streamwise direction are similar to data obtained in a subsonic reattachments behind a rearward facing step[20,21]. The tendency of $\bar{u}$ towards zero, due to the no-slip condition at the wall, takes place on a very short distance, so that the separated profiles have a wake-like shape.

The major part of the profiles behavior between separation and relaxation towards a new flat plate state, far downstream of reattachment, can be represented by a profile family function of a reduced number of parameters[15] (the Reynolds number and a shape parameter, compressibility effects being negligible). This observation is of interest for the development of predictive methods using integral forms of the boundary layer equations[**].

The streamwise variations of the dissipative layer displacement thickness and incompressible shape parameter are represented in Fig. 6.

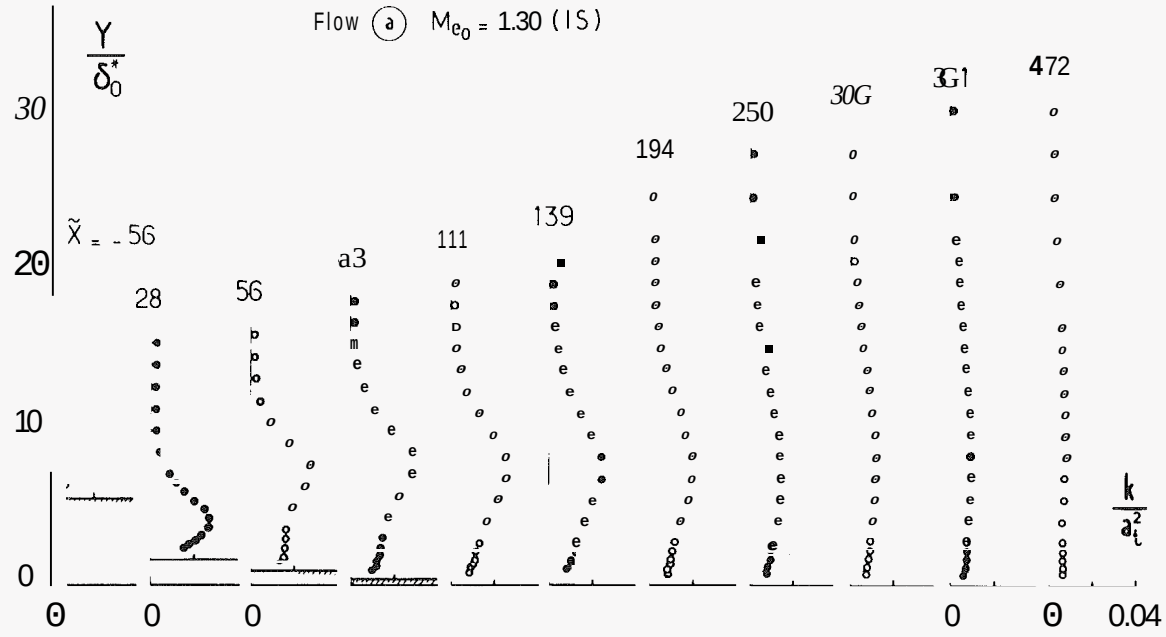

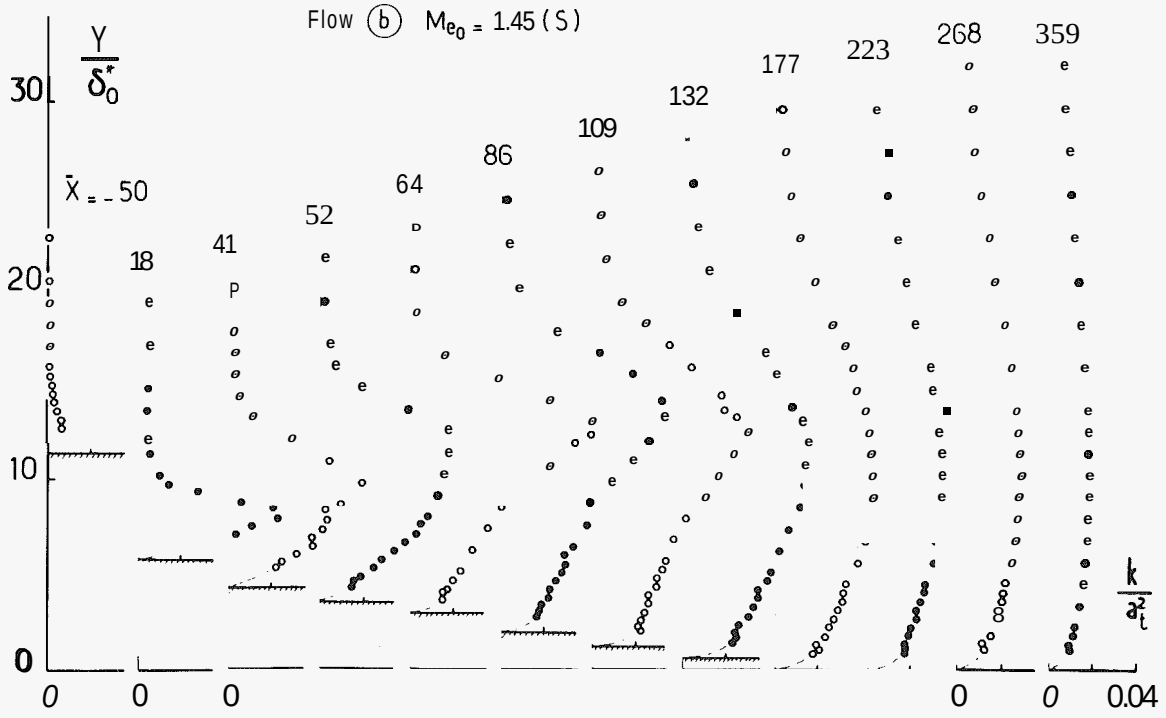

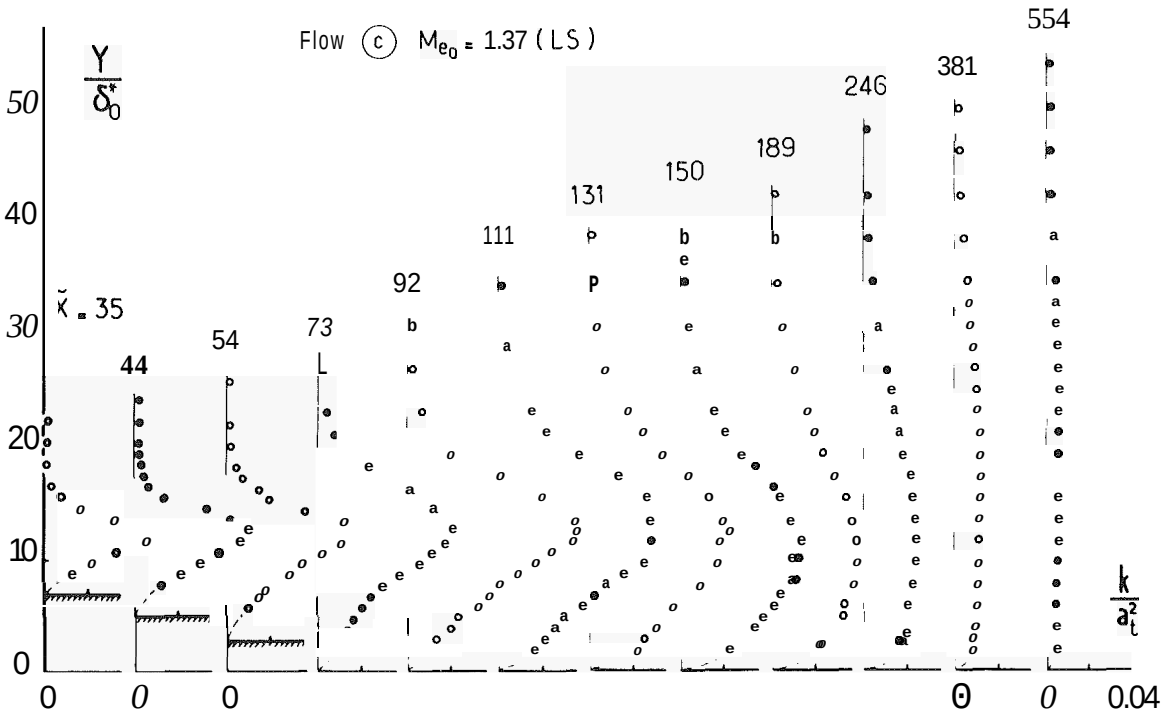

Fig. 7 – Turbulent kinetic energy profiles.

The Initial strong destabilization of the boundary layer entails a very rapid increase of its displacement effect. The shape parameter Hi reaches its maximum value slightly upstream of the maximum of δ^*, this discrepancy being due to the fast growing of the thickness δ. For flow c, Hi reaches very high values (actually not plotted) which correspond to the tendency to a free-shear layer profile. When the reattachment process starts (flows b anc c), one notes a rapid decrease of Hi whose value at the reattachment point R is nearly 3. Downstream of R, Hi relaxes much more slowly towards a flatplate value. (when there is no pressure gradient).

Turbulent Flow Properties

The profiles of turbulence kinetic energy are represented in Fig.7. The kinetic energy k has been evaluated by the formula : $k = (\langle u' \rangle^2 + \langle v' \rangle^2 + \langle w' \rangle^2)/2$ where $\langle w' \rangle^2$ has been taken equal to $(\langle v' \rangle^2 + \langle w' \rangle^2)/2$. For the three flows, there is a very large increase of k in the first part of the interaction process, near the shock foot. The profiles exhibit an important maximum which is neatly detached from the wall. This behavior is still more pronounced for flows b and c, which are separated. For compressible flows, the Reynolds shear stress is given by $-\bar{\rho}\,\overline{u'v'}$ (assuming that the triple correlation $\overline{\rho' u' v'}$ is negligible). However, in the transonic flows under investigation, the change in $\bar{\rho}$ across the dissipative layer is small, so the distribution of $-\overline{u'v'}/a_t^2$ is nearly the same as $-\bar{\rho}\,\overline{u'v'}/\rho_t a_t^2$. Thus, $-\overline{u'v'}/a_t^2$ can, for practical purposes, be interpreted as the non-dimensional Reynolds shear stress. The $-\overline{u'v'}/a_t^2$ distributions are plotted in Fig. 8. They are also characterized by the existence of a well defined maximum, which is also well detached from the wall. For flows b and c, the maximum values of shear stress and turbulent kinetic energy generally coincide with the location of the maximum mean streamwise velocity gradient $\partial\bar{u}/\partial Y$. Such a coincidence is not observed for flow a in the first part of the interaction. where the maximum of $-\overline{u'v'}$ remains closer to the wall than the maximum of k.

In order to give a more vivid idea of the variations of the turbulent quantities during the interaction process, Fig. 9 shows the streamwise evolutions of maximum turbulent kinetic energy and Reynolds shear stress. There is a very large production of turbulence in the initial part of the phenomenon, near the shock root. This production is enhanced when separation occurs ; then k tends to a maximum level, which is between 8 times and 9 times the initial level in the undisturbed boundary layer. For flows b and c, $(k)_{max}$ starts to decrease upstream of the reattachment point R. Downstream of R, the turbulent kinetic energy diminishes rather slowly and tends gradually to a new equilibrium state. The shear stress grows at a relatively slower pace than k, and reaches its maximum value downstream of the point where k culminates. For separated flows, the location of maximum shear stress coincides pratically with the reattachment point ; there, the shear stress has reached a level which is 10 times the maximum initial value.

In fact, the separating boundary layer, undergoes such an over whelming perturbation that, as Bradshaw[22] postulated, the development of the free shear layer is not significantly influenced by its initial conditions, i.e. the initial boundary layer characteristics, and that production of turbulence continues in proportion to the growth of the large scale structure until reattachment occurs[12].

When a large separated zone develops, there is a rapid tendency of the streamwise velocity component to a behavior similar to that of a free shear layer. This property is well illustrated if ones plots the $\bar{u}$ profiles by using the dimensionless velocity (classical in turbulent jets studies) $\varphi = (\bar{u} - \bar{u}_{rn})/(\bar{u}_e - \bar{u}_{rn})$, where $\bar{u}_m$ is the minimum negative velocity, as a function of the reduced ordinate $\eta = (y - y_{\varphi=0.5})/b$ where b is a conventional mixing zone thickness, defined as $b = (y_{\varphi=0.95} - y_{\varphi=0.5})$. The separated profiles of flow c, thus reduced are represented in Fig. 10. One notices a very good correlation of the experimental points, which define a curve practically identical with the well known theoretical curve of Gortler. The reduced distribution $\langle u' \rangle / \langle u' \rangle_{max}$ exhibits also a rather good correlation which agrees relatively well with incompressible jet data.

However the similitude with a mixing layer is not entire, as can be seen if one considers the behavior of the vertical fluctuations. The streamwsie variation of the maximum RMS values $\langle u' \rangle/a_t$ and $\langle v' \rangle/a_t$ are plotted in Fig. 11. In the upstream part of the interaction, the streamwise fluctuations are seen to exceed the vertical fluctuations by

more than a factor of 3. Similar observations are reported in Refs. 10, **14** in contrast to a mixing layer where $\langle u' \rangle$ is only 30 % higher than $\langle v' \rangle$.

The large increase in $\langle u' \rangle^2$ is to be expected if one considers the production term of the $\langle u' \rangle^2$ transport equation (written here in the case of an incompressible flow) : $P = -2\overline{u'v'}\,\partial\bar{u}/\partial Y - 2\overline{u'^2}\,\partial\bar{u}/\partial X$. In the first part of the interaction process, the term involving the streamwise $\bar{u}$ derivative is as large as the term involving the strain rate $\partial\bar{u}/\partial Y$ (see below) due to the strong retardation of the whole dissipative flow. Thus, P is here the sum of two large positive terms. On the other hand, the production mechanism for $\langle v' \rangle^2$ involves terms whose magnitude is far less important : $P = -2\overline{u'v'}\,\partial\bar{v}/\partial X - 2\overline{v'^2}\,\partial\bar{u}/\partial Y$. The derivative $\partial\bar{v}/\partial X$ is small ; $\partial\bar{u}/\partial Y$ is equal to $-\partial\bar{u}/\partial X$, (nearly equal for weakly compressible flows), so that the second term tends to decrease $\langle v' \rangle^2$ production in the first region where $\partial\bar{u}/\partial X$ is every-where negative. Farther downstream, a larger and larger part of the viscous layer is accelerated, which explains the later growth of $\langle v' \rangle^2$

Furthermore, the shear stress coefficient $(-\rho\,\overline{u'v'})_{max}/\rho_e\,\overline{u_e}^2$ reaches values which are significantly higher than the values for an incompressible mixing zone (0.02 instead of 0.014). Further downstream, $\langle v' \rangle$ is still increasing when $\langle u' \rangle$ has started to diminish, so that $\langle v' \rangle$ reaches its highest level well downstream of the maximum $\langle u' \rangle$ location. Proceeding more downstream $\langle u' \rangle$ and $\langle v' \rangle$ become quite comparable. The maximum fluctuation rates $\langle u' \rangle/\bar{u}_e$ for flows a, b and c are respectively equal to 0.2, 0.32 and 0.38.

Such a strong anisotropy of the flow can play a significant role in the mechanism of turbulence kinetic energy production. For an incompressible flow, and if the term involving the derivative $\partial\bar{v}/\partial X$ is neglected, the production term of the k transport equation writes :

$$P = -\overline{u'v'}\,\partial\bar{u}/\partial y - (\langle u' \rangle^2 - \langle v' \rangle^2)\,\partial\bar{u}/\partial x$$

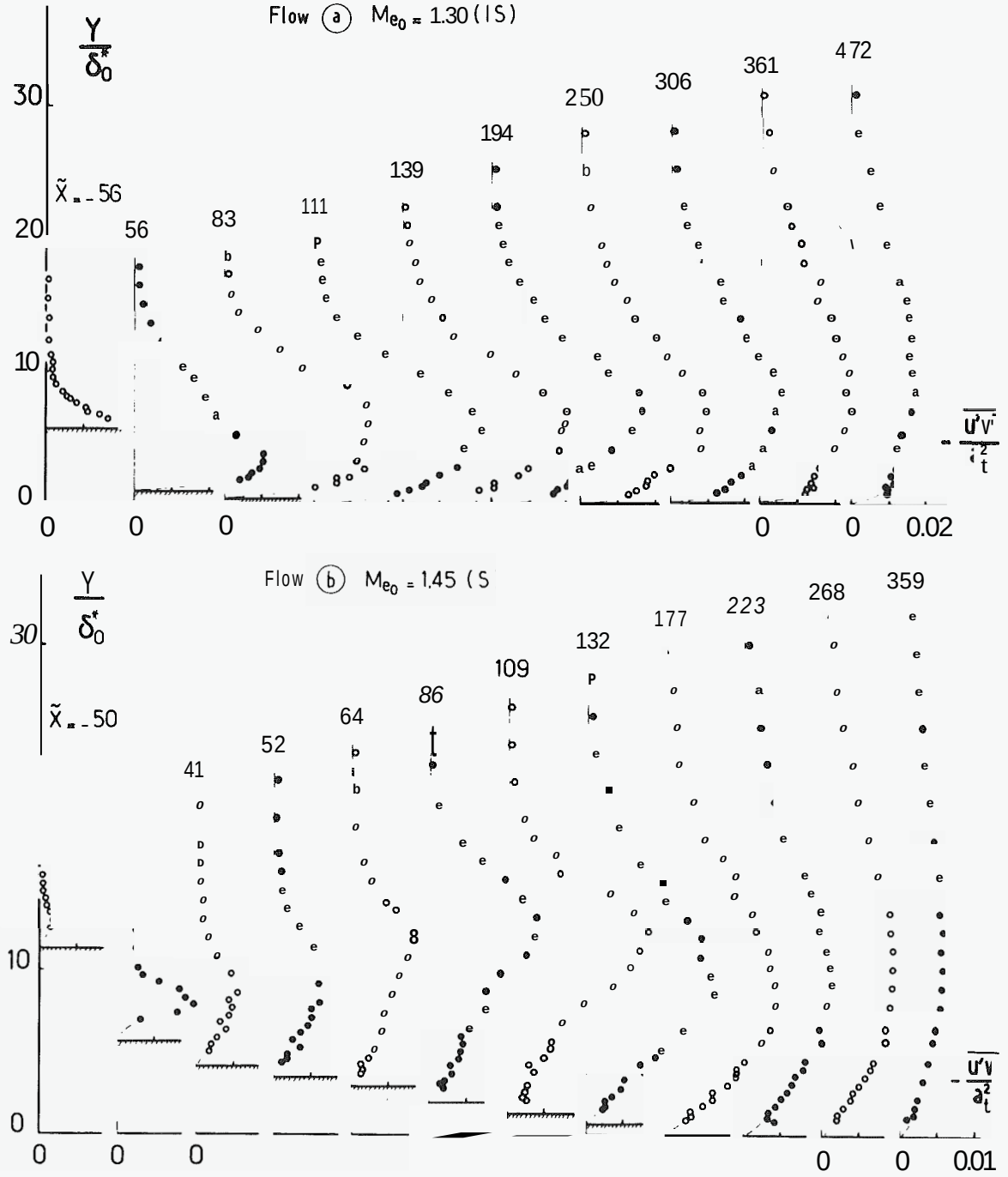

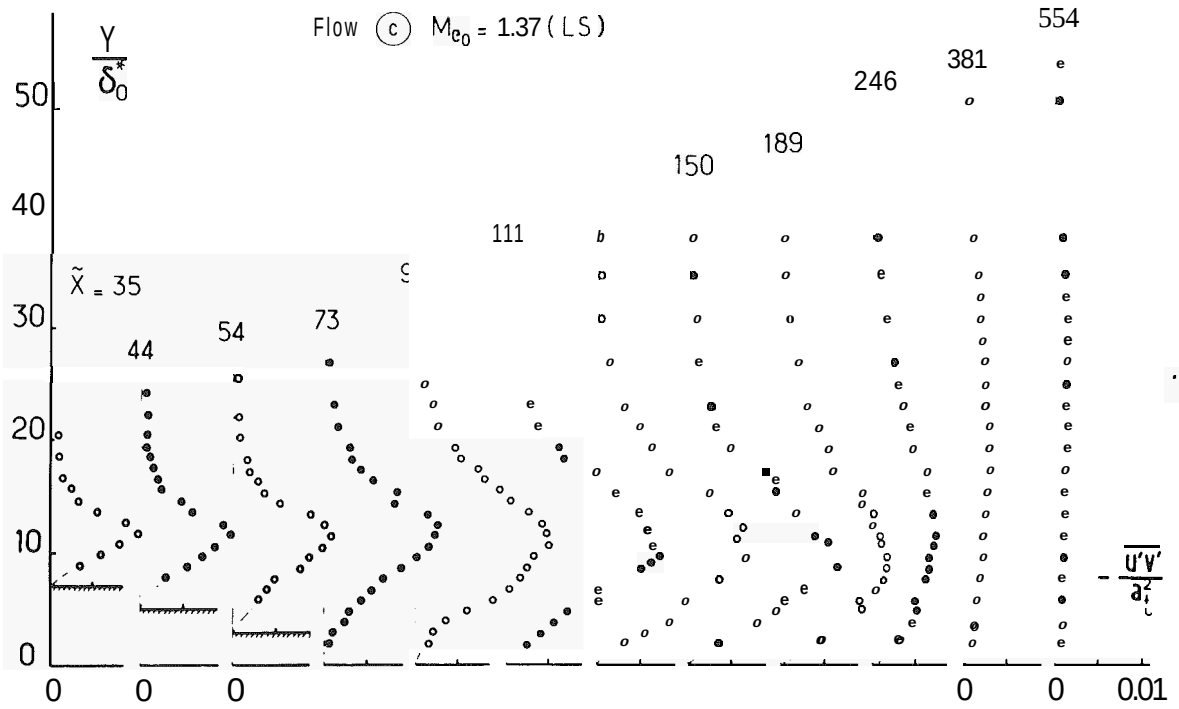

Fig. 8 – Turbulent shear stress profiles.

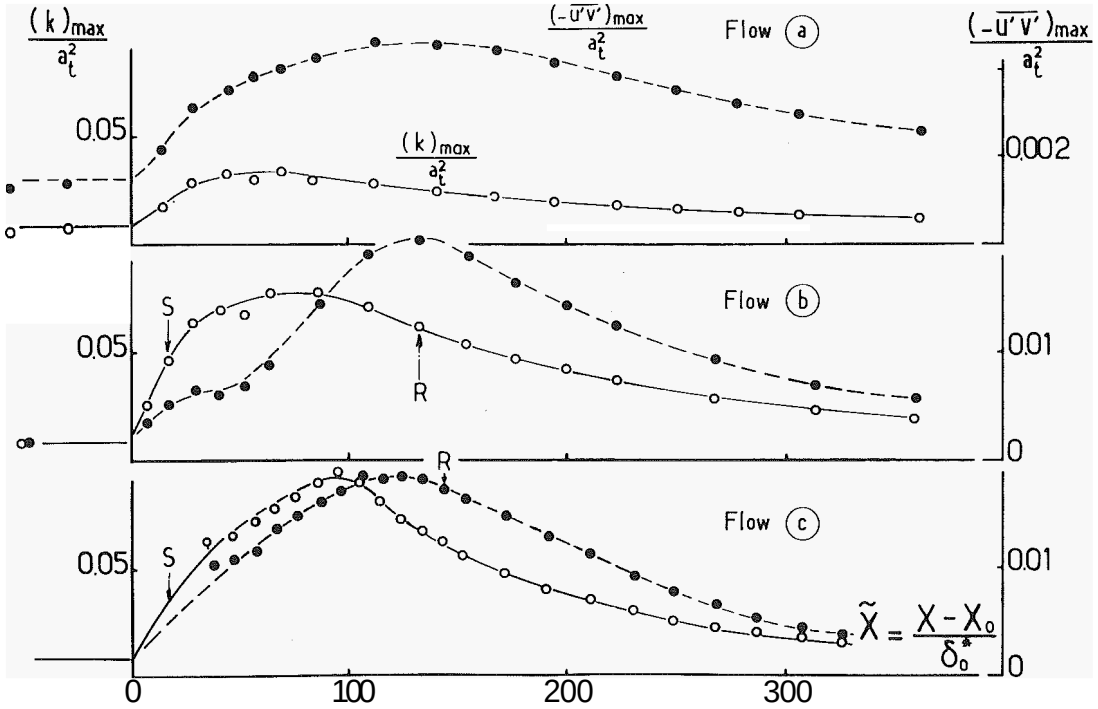

fig. 9 – Maximum kinetic energy and shear stress variation.

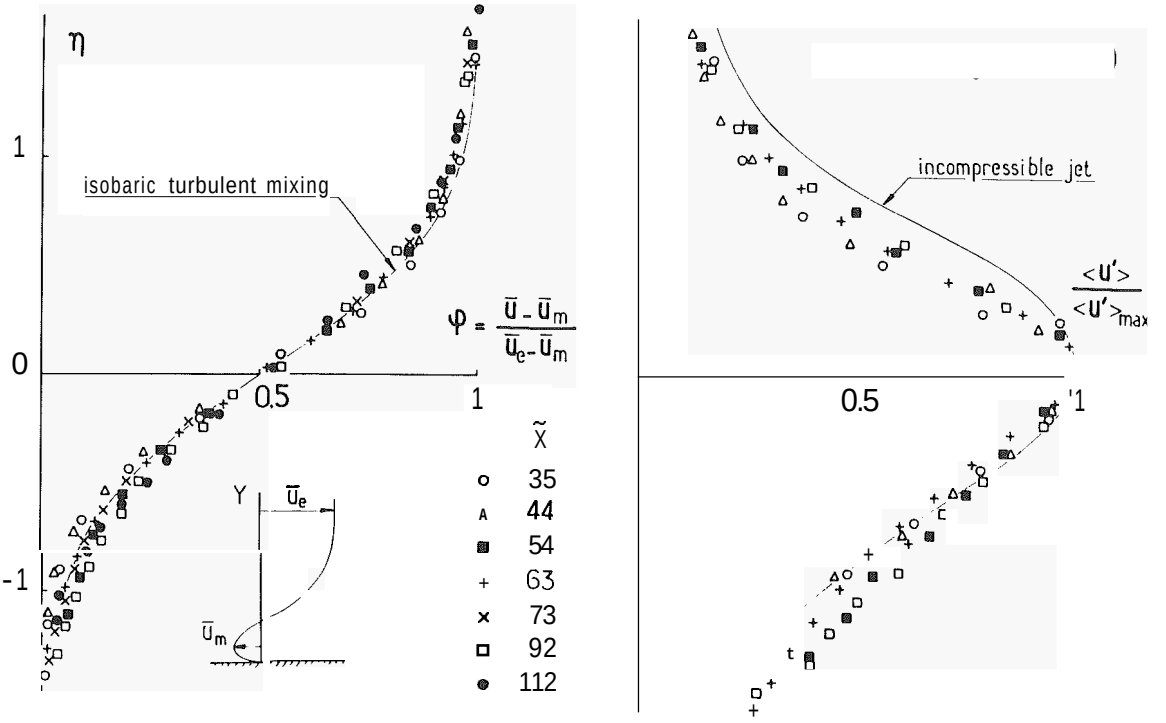

Fig. 10 – Separated zone similarity property.

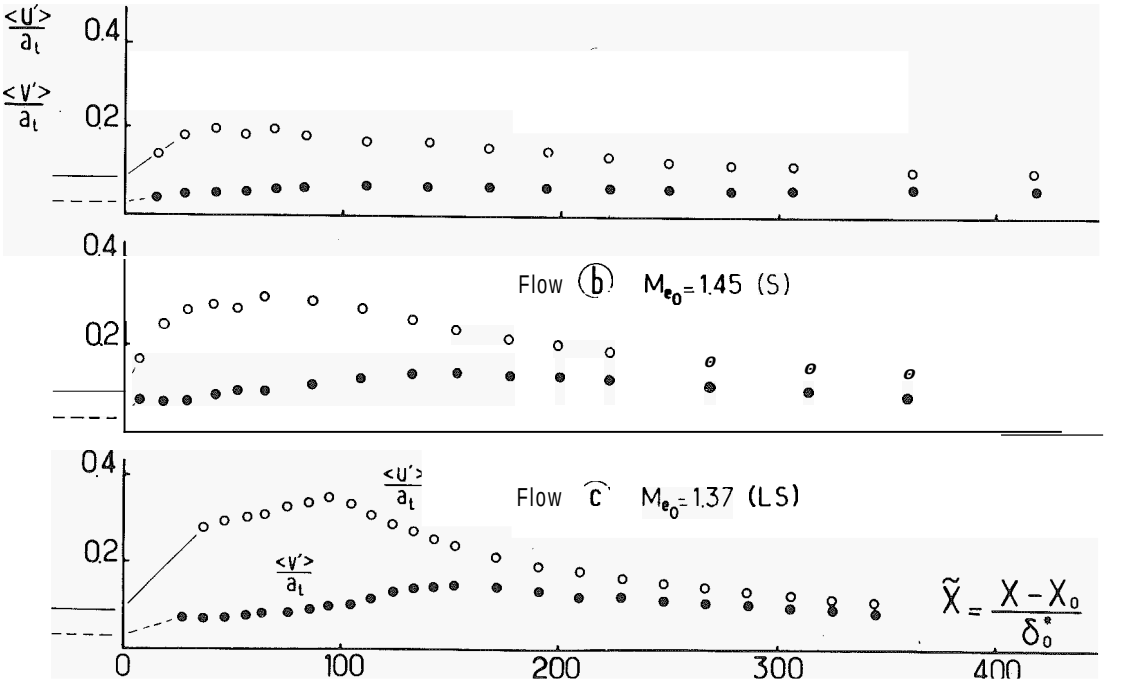

Fg. 11 – Maximum turbulence intensity variation

The first term, representing production by shear stress, is generally predominant in shear layer and/or boundary layer type flows and is frequently only retained in predictive methods. The two production terms have been evaluated for flows a and b for which data in the very first part of the interaction are available. (The calculation has been made after fairing of the experimental values and interpolation by spline functions in order to construct a regular mesh system in the X,Y plane). The results thus obtained are represented in Fig. 12. One notices that production due to normal stresses is as high as production due to shear stress over a streamwise distance which is of the order of 5 δ_0 and which grossly corresponds to the region of steepest axial pressure gradient, where there is a general retardation of the flow ($\partial\bar{u}/\partial X < 0$). Further downstream, the normal stresses contribution becomes rapidly negligible.

Let us now consider another important feature of the flow in the shock region : it is the necessity to take into account the Reynolds normal stresses in the momentum equation. The terms involving Reynolds stresses are, for an incompressible flow :

$$-\partial/\partial Y\ (\overline{u'v'}) - \partial/\partial X\ [\langle u'\rangle^2 - \langle v'\rangle^2]$$

These two derivatives have been evaluated for flows a and b and are plotted in Fig. 13. For these calculations, we have considered the flow as incompressible. This simplification does not change significantly the conclusions because of the small variation of $\bar{\rho}$ across the viscous layer ($\bar{\rho}_e$ /& = 0.83 for M_e = 1) and because of the relatively high uncertainty of this kind of calculations, which involve derivation of experimental data.

It is seen that, in the very first part of the interaction process, the Xderivative of normal stresses can be higher than the shear stress Y-derivative. For the first two streamwise stations, the turbulence level is increasing throughout the dissipative layer, thus leading to a negative term in the momentum equation. Further downstream $\langle u'\rangle^2$ which is far greater than $\langle v'\rangle^2$, in this region, starts to decrease near the wall whereas it continues to grow in the core of the boundary layer, giving an S shape curve for the X-derivative. Relatively far downstream, the normal stresses influence becomes negligible. Simpson et al[23] made similar observations near the separation of an inoompressible turbulent boundary layer and also showed that the neglect of the normal-stress term in the momentum and turbulence energy equations is not justified in this region.

The algebraic mixing length distributions evaluated from Reynolds shear stress and mean streamwise velocity profile measurements are represented in Fig. 14. (only results concerning flows a and c are given here ; the same overall tendency is observed for flow b). It is seen that, at the beginning of the interaction, and in the central part of the layer, the magnitude of l/δ (δ being the local boundary layer thickness) is much lower than the classical limit value (l/δ = 0.09) employed for boundary layer calculation. The same observation is reported in Ref. 12. Large errors in $\partial\bar{u}/\partial y$ can be expected in the outer region of the flow, where $\partial\bar{u}/\partial y$ is small ; however, in this region l/δ exhibits a distinct tendency to increase, as was also observed in Ref. 24. The ratio l/δ, in the core of the flow, increases steadily with increasing downstream distance, and reaches values well in excess of 0.09 for the most down-

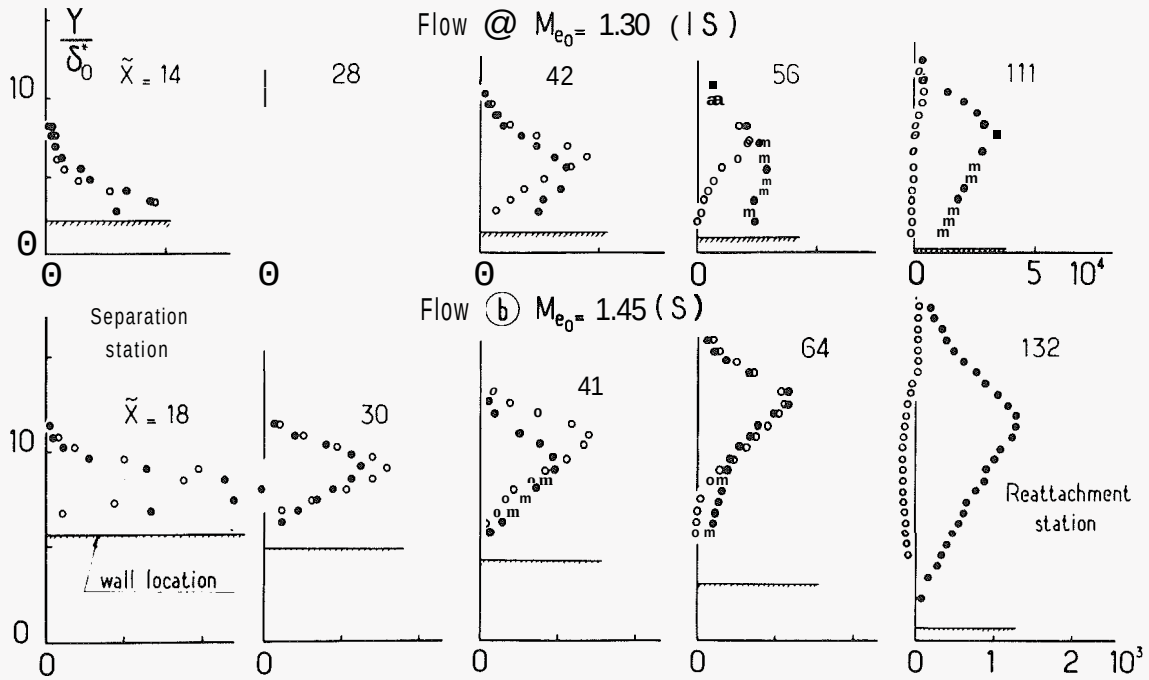

Fig. 12 – Turbulence ***production terms*** ● $-\delta_0^*/a_t^3\ \overline{u'v'}\ \partial\bar{u}/\partial y$ o $-\delta_0^*/a_t^3\ (\langle u'\rangle^2 - \langle v'\rangle^2)\ (\partial\bar{u}/\partial x)$.

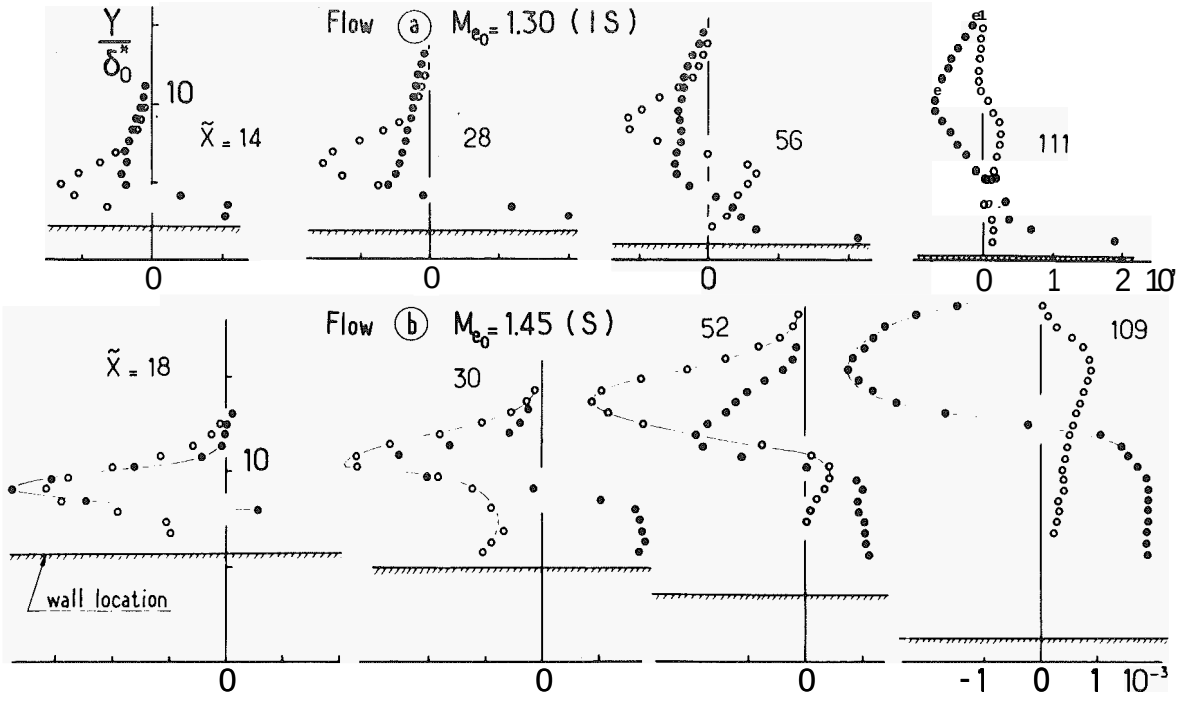

Fig. 13 – Reynolds stress derivatives ● $(\delta_0^*/a_t^2)\,(\partial(-\overline{u'v'})/\partial y)$ o $-(\delta_0^*/a_t^2)\,(\partial/\partial x)(\langle u'\rangle^2 - \langle v'\rangle^2)$

stream station, demonstrating that turbulence has still a structure different from thestructureof an equilibrium flat plate. The inaccuracy of data very near the wall makes it difficult to interpret with confidence the experiments in this region. The high values of l/δ found near the wall at stations $\tilde{X}$ = 44 and $\tilde{X}$ = 83 (flow c), correspond to the reversed part of the $\bar{u}$ profile where $\partial\bar{u}/\partial Y$ changes sign.

The whole history of the interacting dissipative layer can be schematically depicted by plotting the square root of the maximum shear stress coefficient C_τ against the equilibrium shape parameter $J = 1 - 1/Hi$. Following East et al. [26], a function G based on the maximum stress can be defined which will be constant for all equilibrium incompressible boundary layer flows and equal to the flat plate value. Thus :

$$G = (Hi - 1)/Hi\sqrt{C_\tau/2} = 6.55$$

specifies the straigth line in Fig. 15. If one plots $\sqrt{C_\tau}$ against J for the present flows, the experimental points fall below the equilibrium locus in the first part of the interaction, indicating that, during this rapid interaction process, there exists a departure from equilibrium characterized by a lag of the shear stress. Then, as a consequence of the continuous increase of C_τ, whereas J passes through a maximum and then diminishes, the corresponding curves bend and cross the equilibrium locus at a point whose location is a function of the intensity of the destabilization process. Thereafter, the points are above the equilibrium locus and reach a new situation of maximum departure from equilibrium. Downstream of this station, and in the absence of external perturbation, (no pressure gradient), the flows relax towards a new equilibrium state. In the course of this process, the representative points follow a common trajectory which leads to the equilibrium locus.

In order to illustrate the highly fluctuating character of the flows analysed. Fig. 16 shows lines of constant value for the probability of u to be negative. These lines have been determined from histograms of the instantaneous measured values of u. (the reader should note that the Y coordinate has been greatly dilated for clarity's sake). One will note that, in the case of flow a, instantaneous negative values exist in a region where the mean streamwise velocity is positive. This fact may lead to some difficulties in the definition of a turbulent incipient separation situation. This question has been discussed in detail in Ref. **23** where a distinction is suggested between a fully developed separation (or time averaged separation) where the average wall shear stress changes sign, and an intermittent separation which could be defined by the condition that P (u < 0) reaches the values 0.2 near the wall, a condition which is met by flow a. For flowsband c, the probability P (u < 0) is never equal to 1 in the reverse part of the flow, which means that u is varying continuously from negative to positive values even in the most separated case.

Comparison with computations

A preliminary theoretical exploitation of the previous experimental results has been essentially made to examine the ability of "classical" turbulence models to predict shock/boundary layer interaction phenomena. The calculation method employed is based on the boundary layer equations which are solved in inverse mode by a finite difference technique", the input data being the measured displacement thickness distribution. The use of Prandtl's equation is of cuurse questionable near the shock root, where the normal pressure gradient is not negligible. However, such calculation methods allow the use of very fine grids without requiring large computer time. So, they can be very useful to test a large variety of turbulence models, the final step of the model adjustment being made with the full Navier-Stokes equations. Examples of inverse mode computations are presented in Fig. 17; they cuncern flow a.

Two classical boundary layer models have been considered :

i) Michel's mixing length model [28],

ii) the k, ε transport equation model, but without the low Reynolds number terms introduced by Jones and Launder. Near the wall, a mixing length hypothesis is made, the transport equation being used when the turbulence Reynolds number has become sufficiently high.

As can be seen on Fig. 17, the two models fail to predict accu-

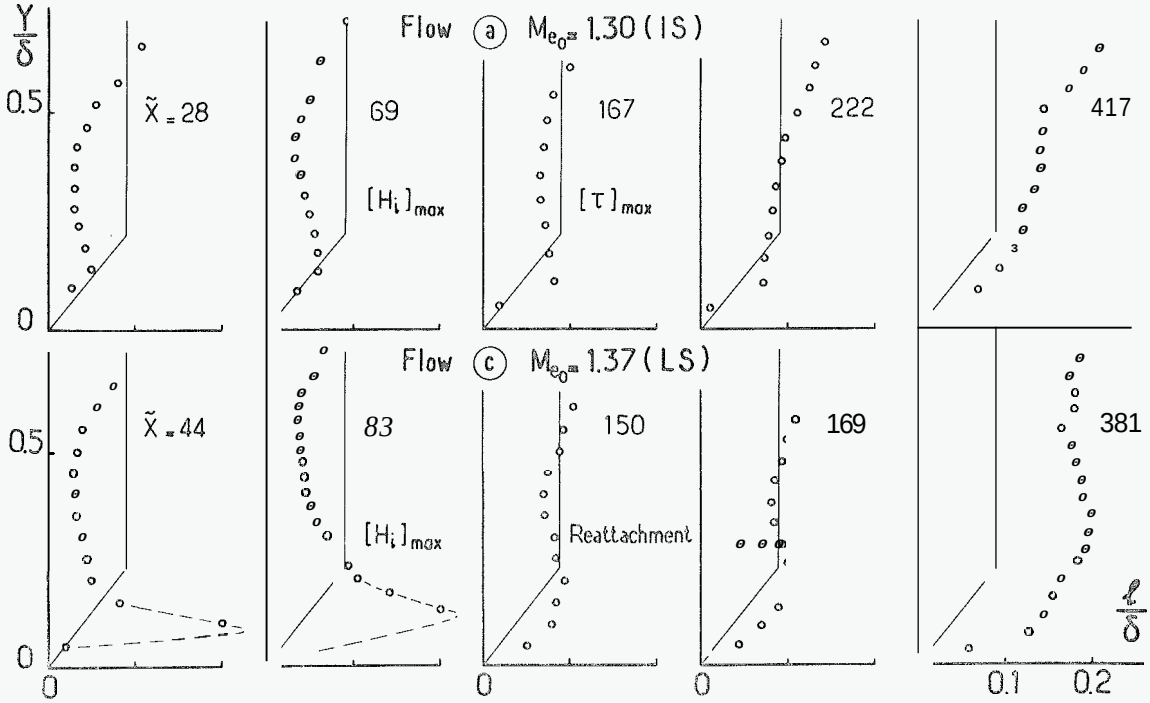

Fig. 14 – Prandtl's mixing length distributions (— Flat plate model).

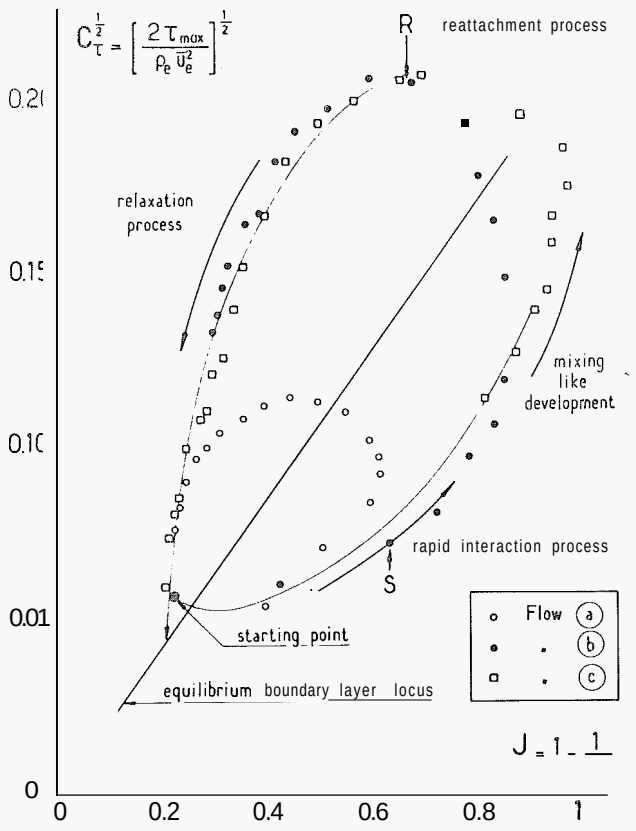

fig. 15 – Evolution of the maximum shear stress with the equilibrium shape parameter.

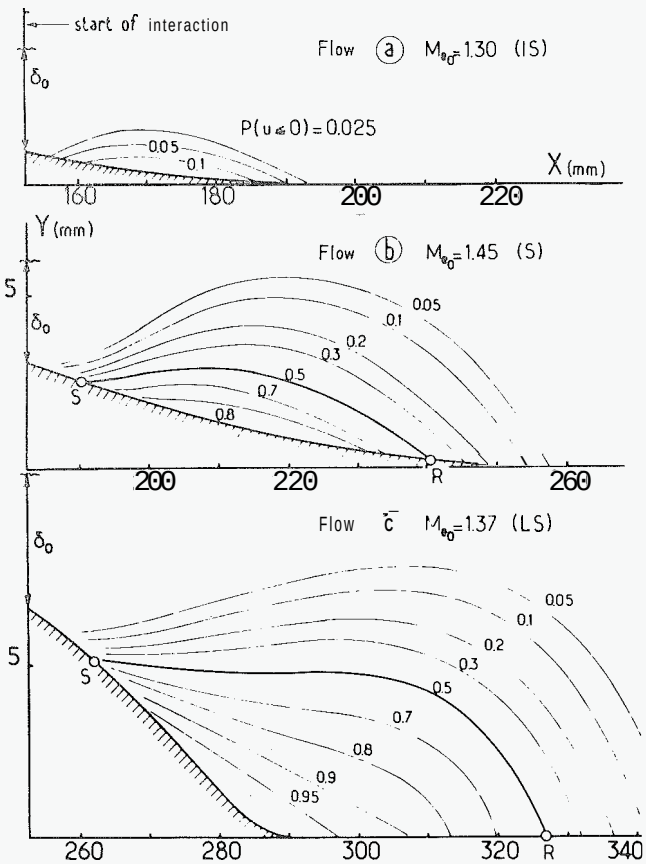

fig. 16 – Lines of constant value for the probability P (u ⩽ 0).

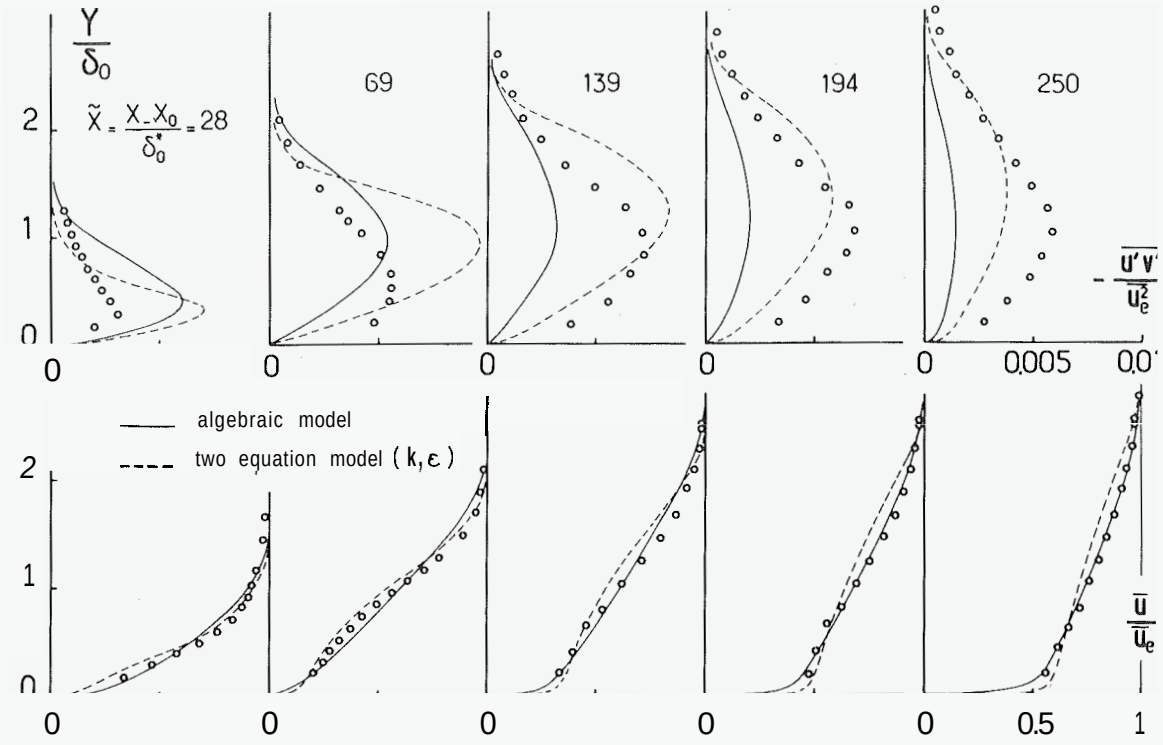

Fig. 17 – Inverse boundary layer computation - Flow a .

rately both velocity profiles and shear stress distributions. They lead to an over prediction of the shear stress level at the interaction beginning, and further downstream they fail to represent the slow relaxation of the turbulent flow. These conclusions had to be expected in view of the previous experimental results. Work is underway with a view to improve multi-equation models, which seem the most appropriate to predict this type of flow.

Conclusion

A study of shock wave-turbulent boundary layer interaction was undertaken in order to provide guidance for turbulence modeling of flows submitted to strong interaction processes. Experiments were performed with the boundary layer developing on the wall of a transonic channel. Three types of flows have been investigated : the first corresponds to an incipient shock induced separation condition, the second to a neatly separated case, the third to a situation where a large separated bubble is formed. These flows have been probed by using a two-color laser velocimeter system allowing the measurement of mean velocity and Reynolds stress tensor components. The inviscid flow structure associated with the largest separation has been carefully established by using holographic interferometry.

The turbulence measurements have shown that the first part of the interaction process, which corresponds to the more intense deceleration effects, entails a very large turbulence production which mainly affect the streamwise velocity component. When separation occurs, this component tends very rapidly to a mixing zone behavior.

Initially, the flow exhibits strong anisotropy, the streamwise fluctuations exceeding the vertical fluctuations by more than a factor of 3. when there is separation. Further downstream the anisotropy of the flow diminishes gradually.

Consequently, the neglect of normal stress terms in the momentum and turbulence energy equation is not justified near the shock root, where the flow is submitted to intense retardation.

During the course of interaction, the turbulent dissipative layer can be strongly out of equilibrium ; one notices two maximum departures from equilibrium conditions, which are situated on each side of the equilibrium locus. The relaxation towards a new downstream equilibrium state is a rather long process due to the long life time of the large structures which formed in the region of more intense turbulence production.

The results of this study strongly suggest that only turbulence models using one or several transport equations are able to correctly represent the dissipative layer behavior. A special attention has to be paid to correctly model the very first stage of the interaction, where a precise prediction of all the Reynolds stresses is essential.

References

1 LE BALLEUR, J.C. "Calcul des écoulements à forte interaction visqueuse au moyen de méthodes de couplage" AGARD CP 291, amputation of Viscous Inviscid Interactions, 1980.

2 VIEGAS, J.R. and COAKLEY, T. J. "Numerical investigation of turbulence models for shock separated boundary layer flows" AIAA Paper 77-44, January 1977.

3 OAKLEY, T.J. , VIEGAS, J.R. and HORSTMAN, C.C. "Evaluation of turbulence models for three type of shock separated boundary layers". AIAA Paper 77-662, June 1977.

4 VIEGAS, J.R. and HORSTMAN, C.C., "Comparison of multi-equation turbulence models for several shock separated boundary layer interaction flows". AIAA Paper 78-1168 (July 1978).

5 COAKLEY, TJ. and BERGMANN, M.Y. "Effects of turbulence model selection on the prediction of complex aerodynamic flows" AIAA Paper 79-0070 (January 1979).

6 MARVIN, J.G., LEVY Jr, L.L. and SEEGMILLER, H.L. "Turbulence modeling for unsteady transonic flows" AIAA Journal, Vol. 18, N°5, May 1980, pp. 489496.

7 ALBER. I.E., BACON, J.W., MASSON, B.S. and COLLINS, D.J. "An experimental investigation of turbulent transonic viscous-inviscid interactions". AIAA Journal, Vol. 11, N° 5, May 1973, pp. 620-627.

8 KOOI, J.W. "Influence of free stream Mach number on transonic shock wave boundary layer interactions". NLR MP 78013 U; 1978.

9 DELERY, J. "Recherches sur l'interaction onde de choc-couche limite turbulente" Rech. Aerosp. N°1977-6. pp. 377-348, English translation ESA-TT 476 (1978).

10 JOHNSON, D.A. "Transonic flow about a two-dimensional airfoil. Inviscid and turbulent flow properties" AIAA Paper 78-1117 (July 1978).

11 ALTSTATT, M.C. "An experimental and analytic investigation of a transonic shock-wave/ boundary layer interaction" AEDC-TR-77-47. May 1977.

12 SEEGMILLER, H.L., MARVIN, J.G., and LEVY Jr, L.L. "Steady and unsteady transonic flow" AIAA Journal, Vol 16, N°12, (Dec. 1978). pp. 1262-1270.

13 JOHNSON, D.A., BACHALO, W.D and OWEN, F.K. "Transonic flow past a symmetrical airfoil ai high angle of attack" J. of Aircraft, Vol. 18, N° 1, January 1981, pp. 7-14.

14 ARDONCEAU, P., LEE, D.H., ALZIARY DE ROQUEFORT, T. and GOETHALS, R. "Turbulence behavior in a shock wave/bar boundary layer interaction", in AGAR9 CP 271, Turbulent boundary layers. Experiments, Theory and Modeling, 1979.

15 DELERY, J. "Analyse du décollement résultant d'une interaction choc-couche limite en transsonique" Rech. Aerosp. N° 1978-6, pp. 305-320, English translation ESA-TT.560.

16 Mc LAIJGHLIN, D.K. and TIEDERMAN, W.G. "Biasing correction for individual realization of laser anemometer measurements in turbulent flows" The Physics of Fluids, Vol. 16, N°12. Dec. 1973.

17 DELERY, J., SURGET, J. et LACHARME J.P. " Interférométrie holographique quantitative en écoulement transsonique bidirnensionnel". Rech. Aérosp. N° 1977-2 p. 89-101 English translation ESA-TT 408 (1977).

18 SIRIEIX, M.. DELERY, J. and STANEWSKY, E. "High Reynolds number boûndary layer shock wave interaction in transonic flow. Cooperative work carried out at DFVLR and ONERA". To be published in Lecture Notes in Physics, Springer Verlag, 1981.

19 CHAPMAN, D.R., KUEHN D.M. and LARSON, H.K. "Investigation on separaied flows in supersonic and subsonic streams with emphasis on the effect of transition" NACA TR 1359 (1958).

20 TANI, I., IUCHI, M. and KOMODU, H. "Experimental investigation of flow separation associated with a step or a groove" Aeronautical Research Institute, University of Tokyo, Rept. N° 364, April 1961 .

21 LE BALLEUR, J.C. and MIRANDE, J. "Experimental and theoretical study of two-dimensional, turbulent, incompressible reattachment "AGARD Meeting on Separated Flows. Gottingen, May 27-30, 1975, pp. 17-1· 17-13 (NASA Technical Translation).

22 BRADSHAW, 2. 2nd WONG, F.Y.F. "The reattachment and relaxation of a turbulent shear layer "Journal of Fluid Mechanics, Vol. 52, pt.I, 1972, pp. 113-135.

23 SIMPSON, R.L., STRICKLAND, J.H. and BARR. P.W. "Features of separating turbulent boundary layer in the vicinity of separation". Journal of Fluid Mechanics, Vol. 79, Pt.3, 1977, pp. 553-594.

24 ETHERIDGE, D.W. and KEMP, P.H. "Measurements of turbulent flow downstream of a rearward-facing **step**" Journal of Fluid Mechanics, Vol. 86, Pt 3, 1978, pp. 545-466.

25 EAST, L.F. et SAWYER, W.G. "An investigation of the structure of equilibrium turbulent boundary layers", in AGARD CP 271, Turbulent boundary layers. Experiments, theory and modelling, 1979.

26 CARTER, J.E. and WORNOM, S.F. "Solution for incompressible separated boundary layers including viscous inviscid interocrion" NASA SP 347 pp. 125-150 (1975).

27 MiCHEL, R., QUEMAXD, C and DURANT, R. "Application d'un schéma de longueur de mélange amélioré à l'étude des couches limites d'bquilibre" ONERA NT 154 (1969).